Infrared photodissociation spectroscopy of $[Al(NH_3)_n]^+$ (n = 1–5): solvation structures and insertion reactions of Al^+ into NH_3

Yutaka Mune [a], Kazuhiko Ohashi [b,*], Takuro Iino [a], Yoshiya Inokuchi [c,1], Ken Judai [c], Nobuyuki Nishi [c], Hiroshi Sekiya [b]

[a] *Department of Molecular Chemistry, Graduate School of Sciences, Kyushu University, Hakozaki, Fukuoka 812-8581, Japan*

[b] *Department of Chemistry, Faculty of Sciences, Kyushu University, Hakozaki, Fukuoka 812-8581, Japan*

[c] *Institute for Molecular Science, Myodaiji, Okazaki 444-8585, Japan*

Abstract

The $[Al(NH_3)_n]^+$ ions with n = 1–5 are studied by infrared photodissociation spectroscopy and density functional theory calculations. The inserted $[H–Al–NH_2]^+$ structure is calculated to be higher in energy than the adduct $[Al–NH_3]^+$ structure. However, incremental solvation stabilizes the inserted structure more efficiently than the adduct structure, because of a larger effective charge on the Al atom in $[H–Al–NH_2]^+$. Actually, the infrared spectra demonstrate that the $[(H–Al–NH_2)(NH_3)_{n-1}]^+$ ions are predominant over $[Al–(NH_3)_n]^+$ for $n \geq 4$, while the adduct structures dominate the spectra of $[Al(NH_3)_n \cdot Ar]^+$ for n = 1–3.

---

* Corresponding author. Fax: +81-92-642-2607.

E-mail address: kazu.scc@mbox.nc.kyushu-u.ac.jp (K. Ohashi).

[1] Present address: Department of Basic Science, Graduate School of Arts and Sciences, The

University of Tokyo, Komaba, Meguro-ku, Tokyo 153-8902, Japan.

1. Introduction

The interaction of metal ions with small ligands, e.g. water and ammonia, has been a prototype for considering ion solvation. Gas-phase studies of solvated metal ions have contributed significantly to our understanding of metal–ligand interactions [1]; various mass spectrometric experiments [2] and electronic spectroscopy [3–5] have probed the binding energetics, reactivities, and structures of metal–ligand complexes. Recently, infrared (IR) spectroscopy has been applied to the study of gas-phase ions, providing detailed information on the solvation structures. Lisy et al. [6,7] have extensively studied alkali metal ions solvated with several different ligands. Duncan et al. [8,9] have employed laser-vaporization method to study a number of other metal ions including Mg^+, Ca^+, Al^+, Si^+, and transition metal ions.

The $[Al(NH_3)_n]^+$ system has received less attention compared to $[Al(H_2O)_n]^+$ and $[Mg(NH_3)_n]^+$. Sato et al. [10] studied the reaction of neutral ammonia clusters $(NH_3)_n$ and Al^+ prepared by laser ablation. Theoretical calculations were carried out for $[Al(NH_3)_1]^+$ [11–15] and $[Al(NH_3)_2]^+$ [14] to predict the geometrical structures, binding energies, and vibrational frequencies.

Matrix-isolation IR [16] and ESR [17] studies revealed that the reaction of the *neutral* Al atom with NH_3 gave an insertion product H–Al–NH_2, which was calculated to be the most stable isomer of this system [18]. It is interesting, therefore, to consider whether such an insertion reaction occurs also in the ionic Al^+–NH_3 system. In relation to this issue, Bowers et al. [19] explored the possibility of Al^+ insertion into H_2 by equilibrium mass spectrometry and ab initio calculations. Hrušák et al. [20] pointed out that the $[Al–H_2O]^+$ adduct is more stable than the inserted $[H–Al–OH]^+$ isomer and a significant barrier exists between them. However, Watanabe and Iwata [21] showed that successive hydration stabilizes the $[H–Al–OH]^+$ unit more efficiently than the Al^+ ion. Indeed, Inokuchi et al. [22] obtained evidence of the inserted $[(H–Al–OH)(H_2O)]^+$ structure by the IR spectroscopy of $[Al(H_2O)_2]^+$.

We reported the IR spectra and solvation structures of $[Mg(NH_3)_n]^+$ previously [23]. In this work, we turn our attention to $[Al(NH_3)_n]^+$. The results of the Al^+ ($3s^2$) complexes are

compared with those of the Mg^+ ($3s^1$) complexes; the comparison allows us to explore the effect of changing the occupation of the 3s orbital on the solvation structures. We also explore the possibility of Al^+ insertion into the NH_3 molecule and the influence of the insertion reaction on the coordination structures.

2. Experimental and computational

The IR photodissociation spectra of $[Al(NH_3)_n]^+$ are measured by using a triple quadrupole mass spectrometer [24]. A mixture of ammonia and argon is expanded through a pulsed nozzle. The second harmonic of a Nd:YAG laser is focused on to a rotating Al rod placed 17 mm downstream of the nozzle; vaporized Al^+ ions are picked up by neutral ammonia clusters in the expansion. The first quadrupole mass filter isolates the parent ions solvated with a particular number of ammonia molecules. After deflection through right angle by an ion bender, the ions are introduced into the second quadrupole ion guide and overlapped with the output of an IR laser (Continuum, Mirage 3000). The vibrational excitation induces fragmentation of the parent ions. The fragment ions are analyzed by the third quadrupole mass spectrometer. The spectra of $[Al(NH_3)_n]^+$ are obtained by recording the yields of the $[Al(NH_3)_{n-1}]^+$ fragment ions as a function of wavenumber of the IR laser.

The energy of a photon in the 2700–3700 cm^{-1} region (32–44 $kJmol^{-1}$) is much smaller than the Al^+–NH_3 bond dissociation energy (≈140 $kJmol^{-1}$) [11–15]. Nevertheless we believe that one-photon absorption predominantly contributes to the spectra, since the IR laser is not focused in the present experiment. This means that we preferentially detect a hot subset of the clusters with internal energies sufficient to break the Al^+–NH_3 bond following one-photon absorption. As a result, the spectral features of smaller clusters are fairly broad due to overlapping hot bands, which preclude a detailed analysis of the spectra. In such a case, we employ “rare-gas tagging” technique, where the spectra of $[Al(NH_3)_n \cdot Ar]^+$ are measured by monitoring the Ar loss channel. The technique is capable of reducing the internal energies of the clusters and decreasing bandwidths without introducing significant spectral shifts.

Density functional theory (DFT) calculations are carried out with GAUSSIAN 98 program package [25]. Since the main purpose here is to predict the theoretical IR spectra of $[Al(NH_3)_n]^+$, no attempt is made to locate *all* the possible isomers at *high* levels of theory. Actually, the geometries of $[Al(NH_3)_n]^+$ are optimized using the B3LYP functionals with 6-31+G* basis sets; the vibrational frequencies and IR absorption intensities are evaluated for a number of typical isomeric structures. The harmonic frequencies are scaled with a factor of 0.9569, which is chosen to reproduce the NH stretching frequency (ν_3 = 3444 cm^{-1}) of the gas-phase ammonia molecule.

3. Results and discussion

3.1. Adduct and inserted structures

Fig. 1 summarizes the structures of $[Al(NH_3)_n]^+$ (n = 1–5) optimized at the B3LYP/6-31+G* level. To our knowledge, only 1I and 2I were treated in the previous theoretical studies [11–15]. In addition to 1I, structure 1II is found for the n = 1 ion (Fig. 1a). In 1I, the Al^+ ion is bonded to the nitrogen atom of ammonia, forming an adduct complex. In 1II, on the other hand, the Al^+ ion is inserted into an NH bond of ammonia. The labels I and II are used hereafter to classify the structures into adduct and inserted types, respectively. The natural charge on the Al atom in 1I is +0.94 while it is +1.84 in 1II; the inserted structure 1II has a character of $H–Al^{2+}–(NH_2)^-$. Our calculations also predict that 1I is by 101 $kJmol^{-1}$ more stable than 1II. The IR photodissociation spectrum of $[Al(NH_3)\cdot Ar]^+$ is consistent with the more stable structure 1I.

3.2. The n = 2 and 3 ions

Structures 2I and 2II are obtained for n = 2 (Fig. 1b). The adduct structure 2I is bent, where two ammonias are located on the same side of Al^+ to avoid the valence electrons localized on the other side. Bent structures of this type are common to the $Al^+(ligand)_2$ and $Mg^+(ligand)_2$ ions [26,27]. In 2II, the second ammonia is bonded to the Al atom in the $[H–Al–NH_2]^+$ subunit. The adduct structure 2I is calculated to be by 38 $kJmol^{-1}$ *less* stable

than the inserted structure 2II; the relative stability of the adduct and inserted structures is reversed between n = 1 and 2.

In Fig. 2, a comparison is made between the experimental spectra of the n = 2 ion and the theoretical spectra of 2I and 2II. The spectrum of $[Al(NH_3)_2]^+$ (Fig. 2a) shows unresolved features spanning from 3100 to 3600 cm^{-1}. The broad features collapse into two sharp bands peaked at 3265 and 3355 cm^{-1} in the spectrum of $[Al(NH_3)_2 \cdot Ar]^+$ (Fig. 2b). The theoretical spectrum of 2II (Fig. 2d) exhibits the symmetric and asymmetric stretches of the NH_2 moiety at 3395 and 3475 cm^{-1}, respectively, in addition to the NH_3 stretches at lower frequencies. The spectrum of $[Al(NH_3)_2 \cdot Ar]^+$ shows no absorption in the region of the asymmetric NH_2 stretch (3475 cm^{-1}), indicating that 2II is absent in the cold subset of the ions provided by the Ar-tagging method. On the other hand, the theoretical spectrum of 2I (Fig. 2c) nicely reproduces the experimental spectrum; the transitions in the 3366–3369 cm^{-1} region correspond to the 3355 cm^{-1} band and the transitions around 3261 cm^{-1} to the 3265 cm^{-1} band.

Fig. 1c shows two typical structures of the n = 3 ion, where all the ligands are directly bonded to the Al^+ ion. Structure 3I is a trigonal pyramidal, which is similar to the structure of $[Mg(NH_3)_3]^+$ [23,27–29]. Again the adduct structure follows the same binding pattern as the Mg^+ complex, where all the ligands are located on the same side of the metal. From our calculations, the adduct structure 3I is by 125 $kJmol^{-1}$ less stable than the inserted structure 3II; the energy difference between the two structures becomes large with increasing n from 2 to 3.

In Fig. 3, the experimental spectra of the n = 3 ion are compared with the theoretical spectra of 3I and 3II. In the spectrum of 3II (Fig. 3d), five distinct transitions are scattered over the 3270–3480 cm^{-1} region. On the other hand, all the prominent transitions are centered around 3370 cm^{-1} in the spectrum of 3I (Fig. 3c). The experimental spectrum of $[Al(NH_3)_3 \cdot Ar]^+$ (Fig. 3b) exhibits only a single band at 3360 cm^{-1}, suggesting the predominant population of the adduct structure 3I. The corresponding band is substantially wide in the spectrum of hot $[Al(NH_3)_3]^+$ (Fig. 3a) and shoulders appear on both sides of the band. These shoulders seem to be due to 3II, which may coexist in the hot subset of the clusters.

The Ar-tagging experiments demonstrate that the adduct structures 2I and 3I are produced exclusively, although they are less stable than the corresponding inserted structures 2II and 3III. In our ion source of pick-up type, the nascent $[Al(NH_3)_n]^+$ ions probably take the adduct forms. The inserted structures are preferable energetically, but we expect a significant activation barrier for isomerization of the adduct to the inserted structures, as reported for the $[Al(H_2O)]^+$ system [20]. The $[Al(NH_3)_2 \cdot Ar]^+$ and $[Al(NH_3)_3 \cdot Ar]^+$ ions are likely to be trapped in local minima corresponding to the adduct structures. The mechanism of cluster formation rather than the energetics leads to the observation of these structures.

3.3. The n = 4 ion

Fig. 1d represents the structures of $[Al(NH_3)_4]^+$. In the adduct structure 4I, two ammonias in 3I are bridged by the fourth one through hydrogen bonds. We cannot find stable structures with the coordination number of four, although such structures are possible for $[Mg(NH_3)_4]^+$ [23,27–29]. In the inserted structure 4II, on the other hand, three ammonias are bonded to the Al atom in the $[HAlNH_2]^+$ subunit.

For the ions with $n \geq 4$, we are only able to measure the spectra without Ar tagging. Fig. 4 shows the spectrum of $[Al(NH_3)_4]^+$ together with the theoretical spectra of 4I and 4II. The most intense transition of 4I is located at 3207 cm^{-1} (Fig. 4b), which is due to the hydrogen-bonded NH stretch. The experimental spectrum (Fig. 4a) shows very weak and broad absorption in the corresponding region (3000–3250 cm^{-1}), suggesting that 4I is present as a minor isomer. On the other hand, the spectrum of the inserted structure 4II coincides well with the main features of the experimental spectrum; the transitions in the 3385–3406 cm^{-1} region correspond to the 3365 cm^{-1} band while the 3286 and 3289 cm^{-1} transitions to the 3300 cm^{-1} band. Thus the IR spectroscopy reveals that the inserted structure is predominant over the adduct structure at $n = 4$.

3.4. Solvation-induced insertion reaction

The Ar-tagging experiments indicate that the adduct structures 1I, 2I, and 3I are

predominant in cold ensembles of the clusters. As mentioned in section 3.2, activation barriers probably prevent the isomerization to the lower-energy structures 2II and 3II. In the experiments without Ar tagging, these inserted structures may coexist, because a part of the clusters in hot ensembles may have internal energies large enough to overcome the barriers. Unfortunately, the substantially broad features in the spectra of n = 1–3 preclude the definitive identification of the inserted structures. In contrast, the spectrum of $[Al(NH_3)_4]^+$ indicates that the inserted structure 4II is predominant over the adduct structure 4I. The observation can be rationalized as follows. The Al atom of the $[H–Al–NH_2]^+$ subunit in the inserted structures has a larger effective charge than that in the adduct structures, as demonstrated for 1I and 1II in section 3.1; the binding of an additional ammonia to the $[H–Al–NH_2]^+$ subunit is stronger than the binding to the intact Al^+ ion in the adduct structures. Therefore, the inserted structures are stabilized more efficiently than the adduct structures by the incremental addition of the solvent molecules. The isomerization barriers, as well as the energy levels of the products, are expected to be lowered with increasing the number of ammonia molecules. Consequently, the nascent adduct structure 4I formed in the pick-up source is able to isomerize to the most stable structure 4II through the insertion reaction within the cluster. IR spectroscopic evidence of intracluster insertion reactions has also been reported for $[Si(CO_2)_n]^+$ [30], $[Ni(CO_2)_n]^+$ [31], and $[V(CO_2)_n]^+$ [32].

3.5. The n = 5 ion

Fig. 1e illustrates three inserted structures of $[Al(NH_3)_5]^+$ examined here; we turn our attention to the distribution of ammonia molecules in the first and second solvation shells. The number of the molecules in the second shell is 0, 1, and 2 for 5IIA, 5IIB, and 5IIC, respectively. The adduct structures are not included here, because they are far less stable than structures 5IIA–5IIC.

In Fig. 5, the experimental spectrum of $[Al(NH_3)_5]^+$ is compared with the theoretical spectra of 5IIA–5IIC. The most intense transitions of 5IIB and 5IIC are located below 3000 cm^{-1}; these transitions are due to the NH group involved in the hydrogen bond between

ammonias in the first and second shells. No appreciable absorption is observed in the corresponding region of the experimental spectrum (Fig. 5a), indicating that 5IIB and 5IIC are missing. On the other hand, the theoretical spectrum of 5IIA totally reproduces the main features of the experimental spectrum.

In the inserted structures, at least four ammonia molecules can be directly bonded to the Al atom in the $[H–Al–NH_2]^+$ subunit, in striking contrast to the adduct structures where the first solvent shell is filled with three ammonia molecules.

3.6. Solvation structures

The 3s electron on Mg^+ plays an important role in the progressive solvation processes of $[Mg(H_2O)_n]^+$ and $[Mg(NH_3)_n]^+$. Theoretical calculations [29] show that all the ammonia molecules in $[Mg(NH_3)_n]^+$ are able to occupy the first shell for $n \leq 6$. On the other hand, both the calculations [29] and experiment [33] confirm that the first shell is completed with three water molecules in $[Mg(H_2O)_n]^+$ and further hydration occurs in the second shell through hydrogen bond(s). Water molecules in $[Mg(H_2O)_n]^+$ have to aggregate on one side of Mg^+ to avoid the 3s electron remaining in the vicinity of Mg^+. On the other hand, the 3s electron in $[Mg(NH_3)_5]^+$ and $[Mg(NH_3)_6]^+$ is distributed beyond the first shell, allowing up to six ammonia molecules to fill the first shell.

The valence electron–ligand repulsion is stronger in $[Al(NH_3)_n]^+$ than in $[Mg(NH_3)_n]^+$, because the Al^+ ion has two electrons in the 3s orbital. Indeed, our calculations reveal that the bent angle ($\angle N–M^+–N$, M = Al or Mg) is smaller in $[Al(NH_3)_3]^+$ (87°) than that in $[Mg(NH_3)_3]^+$ (101°); the full occupation of the 3s orbital forces the solvent molecules to be in closer proximity. Because of the bulky 3s orbital, the fourth ammonia in the adduct structures of $[Al(NH_3)_4]^+$ cannot squeeze into the first shell. Instead, the $n = 4$ ion adopts the inserted structure, avoiding the repulsion with the 3s electrons in a different way. In the $[H–Al–NH_2]^+$ subunit, one of the 3s electrons is involved in the H–Al bond and the other is transferred to the nitrogen atom. Once the $[H–Al–NH_2]^+$ subunit is formed, additional solvent molecules no longer need to avoid the valence electrons. Then the inserted

structures have merely to minimize ligand–ligand repulsion by maintaining the ligands as far apart as possible. As a result, H, NH_2, and NH_3 surround the central Al atom in tetrahedral (3II), hexahedral (4II), and octahedral (5IIA) arrangements for n = 3, 4, and 5, respectively.

Rather than the insertion reactions, H-elimination reactions have been considered in the $[Mg(NH_3)_n]^+$ system [29]. The $[MgNH_2]^+$ ion shows a large solvation energy compared to Mg^+ because of a Mg^{2+}–$(NH_2)^-$ character. However, the H-loss products, $[(MgNH_2)(NH_3)_{n-1}]^+$, are not observed experimentally [34]. This is because the successive solvation energies of $[Mg(NH_3)_n]^+$ are as large as those of $[(MgNH_2)(NH_3)_{n-1}]^+$ for n = 5 and 6, as a result of the charge separation into Mg^{2+} and a diffuse electron [29]. Thus the solvation of Mg^+ proceeds without the metal–ligand reaction. On the other hand, the $[H–Al–NH_2]^+$ ion is formed through the insertion reaction in the solvation process of Al^+. Once the insertion reaction occurs, the $[H–Al–NH_2]^+$ subunit is stabilized more efficiently than the Al^+ ion by the incremental addition of ammonia molecules, because the Al atom in the $[HAlNH_2]^+$ subunit has a larger effective charge than the intact Al atom. The resulting structure 5IIA is likely to form the most stable core for further solvation.

Acknowledgement

This work was supported in part by the Joint Studies Program (2004) of the Institute for Molecular Science and the Grant-in-Aid for Scientific Research (No. 17550014) from the Ministry of Education, Culture, Sports, Science, and Technology of Japan.

References

[1] A. W. Castleman Jr., K. H. Bowen, J. Phys. Chem. 100 (1996) 12911.

[2] J. A. Leary, P. B. Armentrout (Eds.), Gas phase metal ion chemistry (special issue), Int. J. Mass Spectrom. 204 (2001) 1–294.

[3] M. A. Duncan, Ann. Rev. Phys. Chem. 48 (1997) 69.

[4] K. Fuke, K. Hashimoto, S. Iwata, Adv. Chem. Phys. 110 (1999) 431.

[5] J. M. Farrar, Int. Rev. Phys. Chem. 22 (2003) 593.

[6] J. M. Lisy, Int. Rev. Phys. Chem. 16 (1997) 267.

[7] G. N. Patwari, J. M. Lisy, J. Chem. Phys. 118 (2003) 8555.

[8] M. A. Duncan, Int. Rev. Phys. Chem. 22 (2003) 407.

[9] N. R. Walker, R. S. Walters, M.-K. Tsai, K. D. Jordan, M. A. Duncan, J. Phys. Chem. A 109 (2005) 7057, and references therein.

[10] T. Kaya, M. Kobayashi, H. Shinohara, H. Sato, Chem. Phys. Lett. 186 (1991) 431.

[11] M. Alcamí, O. Mó, M. Yáñez, J. Mol. Struct. (Theochem) 234 (1991) 357.

[12] M. Sodupe, C. W. Bauschlicher Jr., Chem. Phys. Lett. 181 (1991) 321.

[13] D. Stöckigt, Chem. Phys. Lett. 250 (1996) 387.

[14] T. D. Palma, A. Latini, M. Satta, M. Varvesi, A. Giardini, Chem. Phys. Lett. 284 (1998) 184.

[15] S. Petrie, R. C. Dunbar, J. Phys. Chem. A 104 (2000) 4480.

[16] D. V. Lanzisera, L. Andrews, J. Phys. Chem. A 101 (1997) 5082.

[17] P. H. Kasai, H. Himmel, J. Phys. Chem. A 106 (2002) 6765.

[18] R. D. Davy, K. L. Jaffrey, J. Phys. Chem. 98 (1994) 8930.

[19] P. R. Kemper, J. Bushnell, M. T. Bowers, G. I. Gellene, J. Phys. Chem. A 102 (1998) 8590.

[20] J. Hrušák, D. Stöckigt, H. Schwarz, Chem. Phys. Lett. 221 (1994) 518.

[21] H. Watanabe, S. Iwata, J. Phys. Chem. 100 (1996) 3377.

[22] Y. Inokuchi, K. Ohshimo, F. Misaizu, N. Nishi, Chem. Phys. Lett. 390 (2004) 140.

[23] K. Ohashi, K. Terabaru, Y. Inokuchi, Y. Mune, H. Machinaga, N. Nishi, H. Sekiya, Chem. Phys. Lett. 393 (2004) 264.

[24] Y. Inokuchi, N. Nishi, J. Chem. Phys. 114 (2001) 7059.

[25] M. J. Frisch et al., Gaussian, Inc., Pittsburgh, PA, 1998.

[26] C. W. Bauschlicher, Jr., H. Partridge, J. Phys. Chem. 95 (1991) 9694.

[27] A. Andersen, F. Muntean, D. Walter, C. Rue, P. B. Armentrout, J. Phys. Chem. A 104 (2000) 692.

[28] S. Yoshida, K. Daigoku, N. Okai, A. Takahata, A. Sabu, K. Hashimoto, K. Fuke, J.

Chem. Phys. 117 (2002) 8657.

[29] K. Daigoku, K. Hashimoto, J. Chem. Phys. 121 (2004) 3569.

[30] J. B. Jaeger, T. D. Jaeger, N. R. Brinkmann, H. F. Schaefer, M. A. Duncan, Can. J. Chem. 82 (2004) 934.

[31] N. R. Walker, R. S. Walters, G. A. Grieves, M. A. Duncan, J. Chem. Phys. 121 (2004) 10498.

[32] N. R. Walker, R. S. Walters, M. A. Duncan, J. Chem. Phys. 120 (2004) 10037.

[33] Y. Inokuchi, K. Ohshimo, F. Misaizu, N. Nishi, J. Phys. Chem. A 108 (2004) 5034.

[34] S.Yoshida, N. Okai, K. Fuke, Chem. Phys. Lett. 347 (2001) 93.

Figure Captions

Fig. 1. Stable structures of $[Al(NH_3)_n]^+$ with (a) $n = 1$, (b) $n = 2$, (c) $n = 3$, (d) $n = 4$, and (e) $n = 5$ obtained from DFT calculations at the B3LYP/6-31+G* level. Aluminum and nitrogen atoms are denoted by solid and hatched circles, respectively. Labels I and II are used to classify the structures into adduct and inserted types, respectively.

Fig. 2. Comparison of experimental IR spectra of (a) $[Al(NH_3)_2]^+$ and (b) $[Al(NH_3)_2 \cdot Ar]^+$ with theoretical IR spectra obtained from DFT calculations for (c) 2I and (d) 2II.

Fig. 3. Comparison of experimental IR spectra of (a) $[Al(NH_3)_3]^+$ and (b) $[Al(NH_3)_3 \cdot Ar]^+$ with theoretical IR spectra obtained from DFT calculations for (c) 3I and (d) 3II.

Fig. 4. (a) Experimental IR spectrum of $[Al(NH_3)_4]^+$ together with theoretical IR spectra for (b) 4I and (c) 4IIB. Intensity of the spectrum of 4II is magnified by a factor of 3.

Fig. 5. (a) Experimental IR spectrum of $[Al(NH_3)_5]^+$ together with theoretical IR spectra for (b) 5IIA, (c) 5IIB, and (d) 5IIC. Intensity of the spectrum of 5IIA is magnified by a factor of

50.

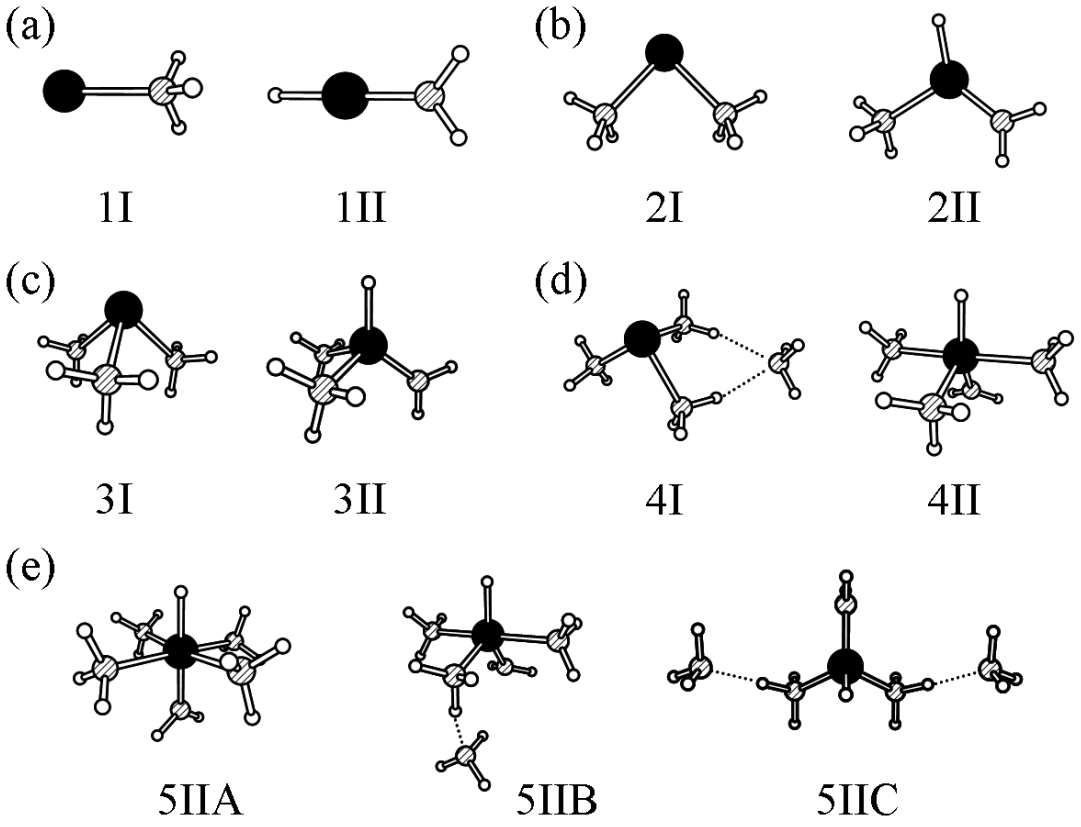

Fig. 1 Mune et

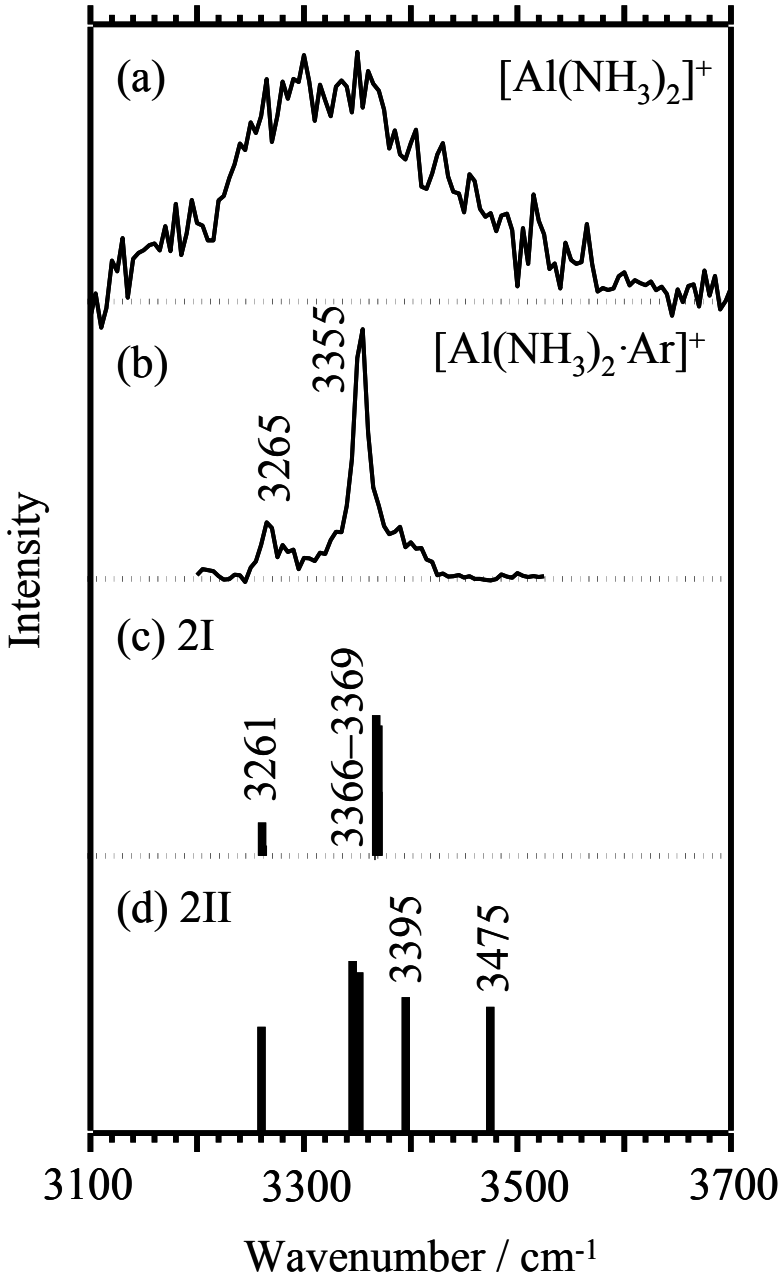
(a)
$[Al(NH_3)_2]^+$
(b)
$[Al(NH_3)_2 \cdot Ar]^+$
3355
3265
(c) 2I
3366–3369
3261
(d) 2II
3395
3475
Intensity
3100
3300
3500
3700
Wavenumber / cm^{-1}

Fig. 2 Mune et

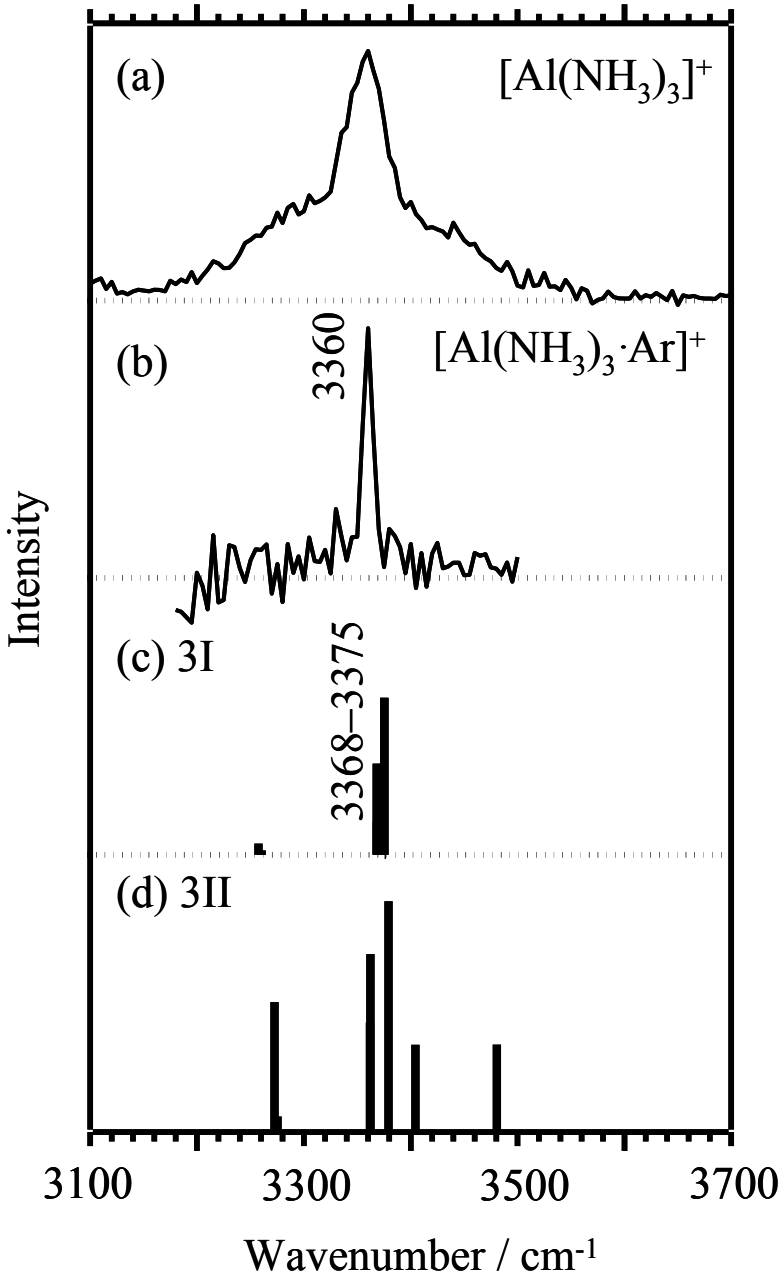

Fig. 3 Mune et al.

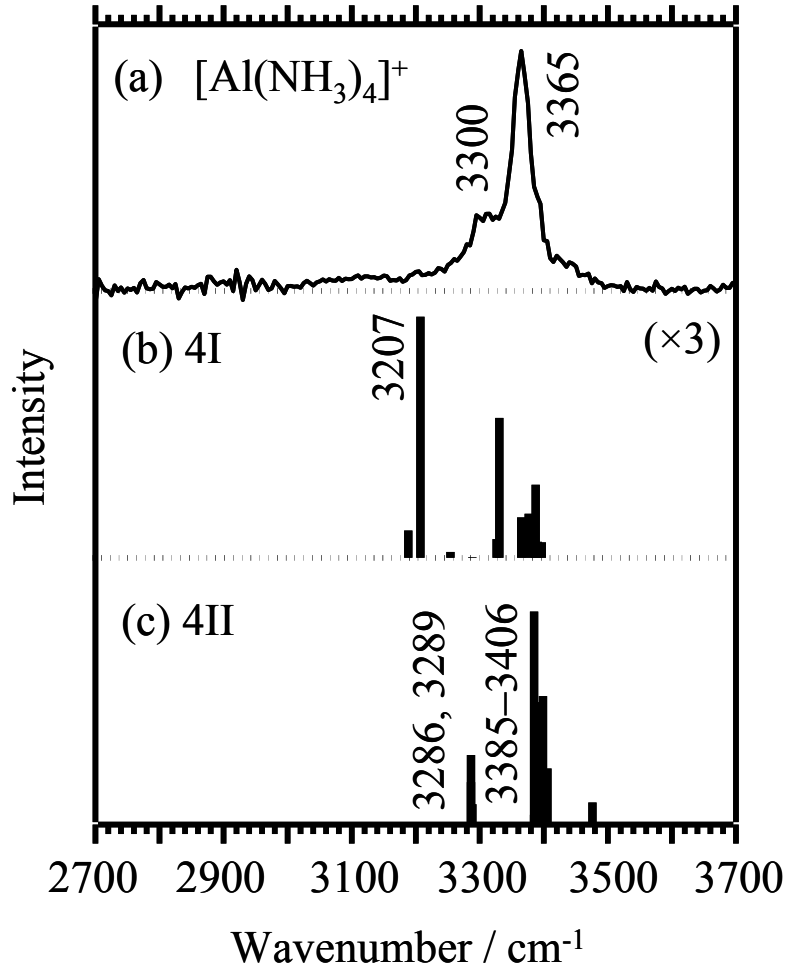

Fig. 4 Mune et al.

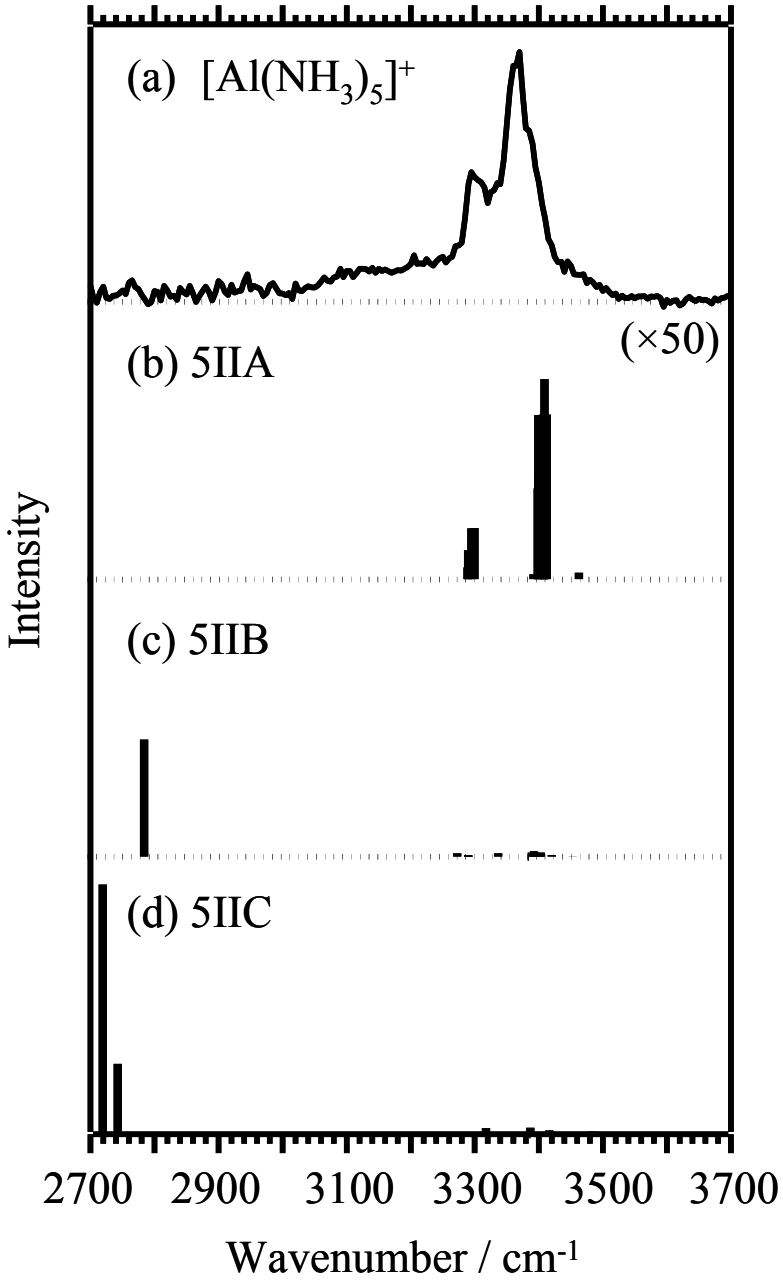

Fig.5 Mune et al.

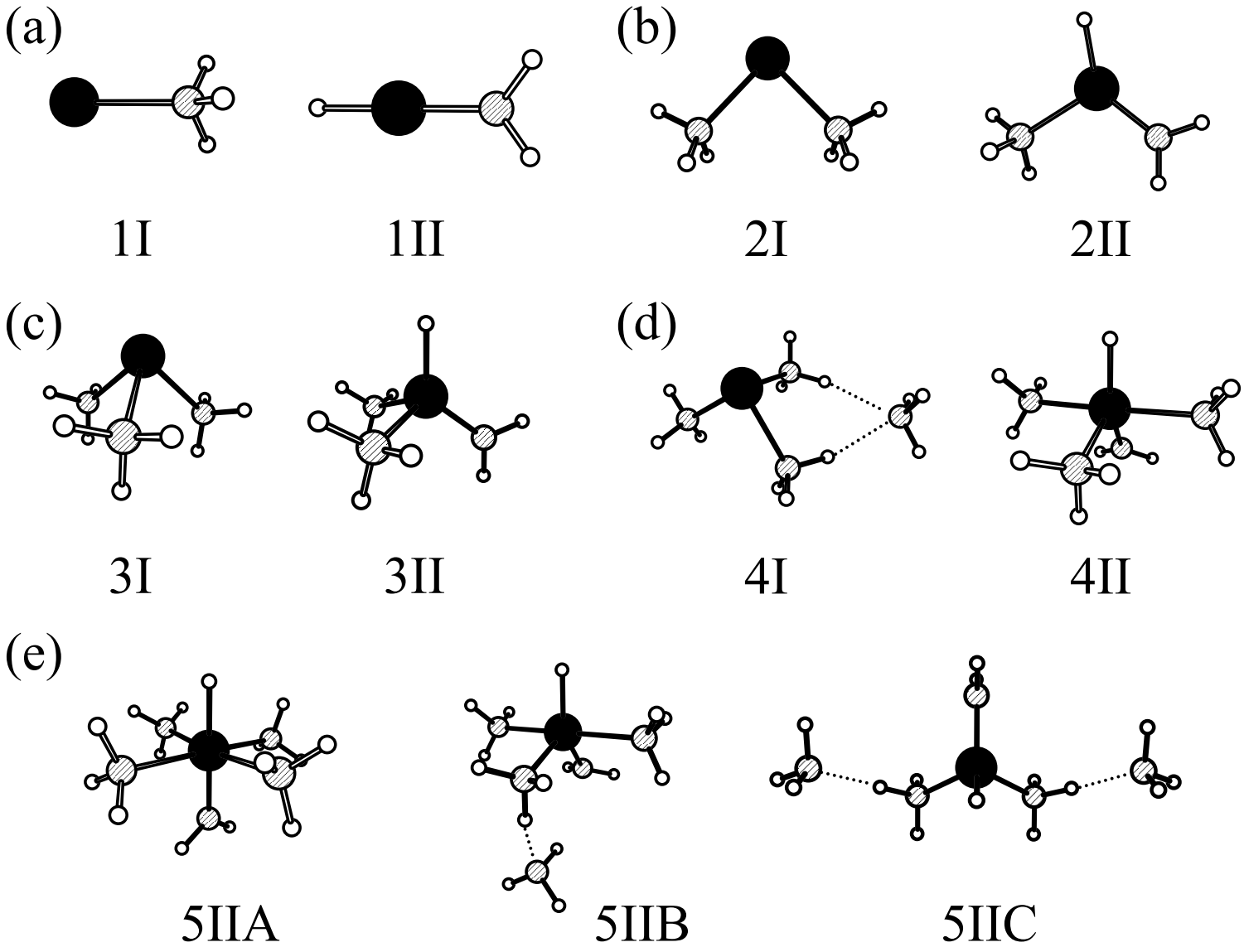

Fig. 1 Mune et al.

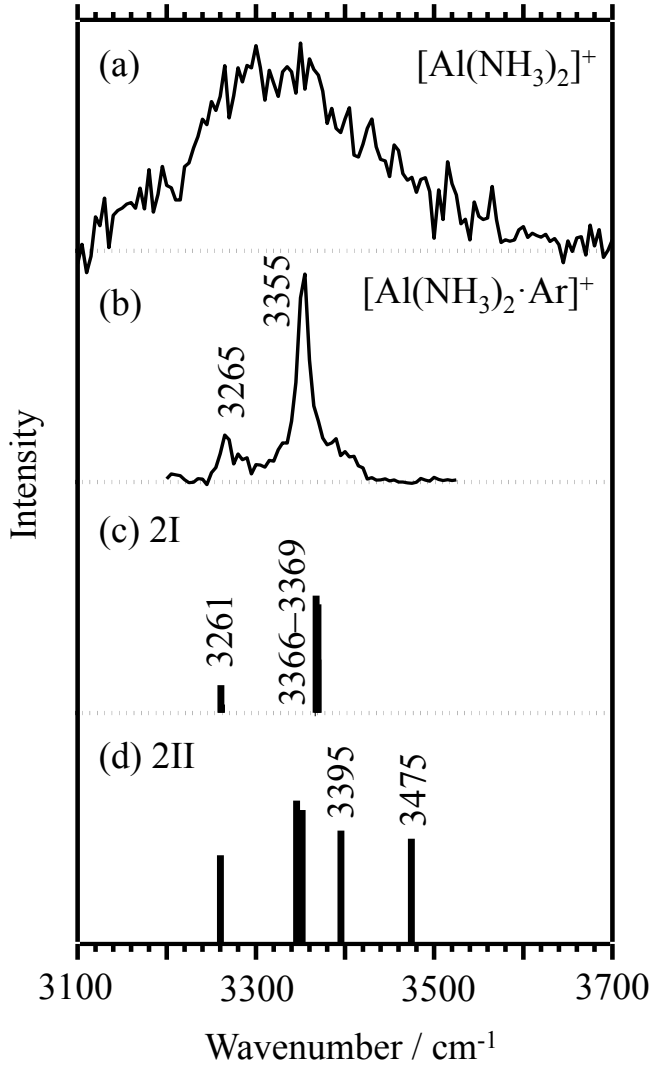

Fig. 2 Mune et al.

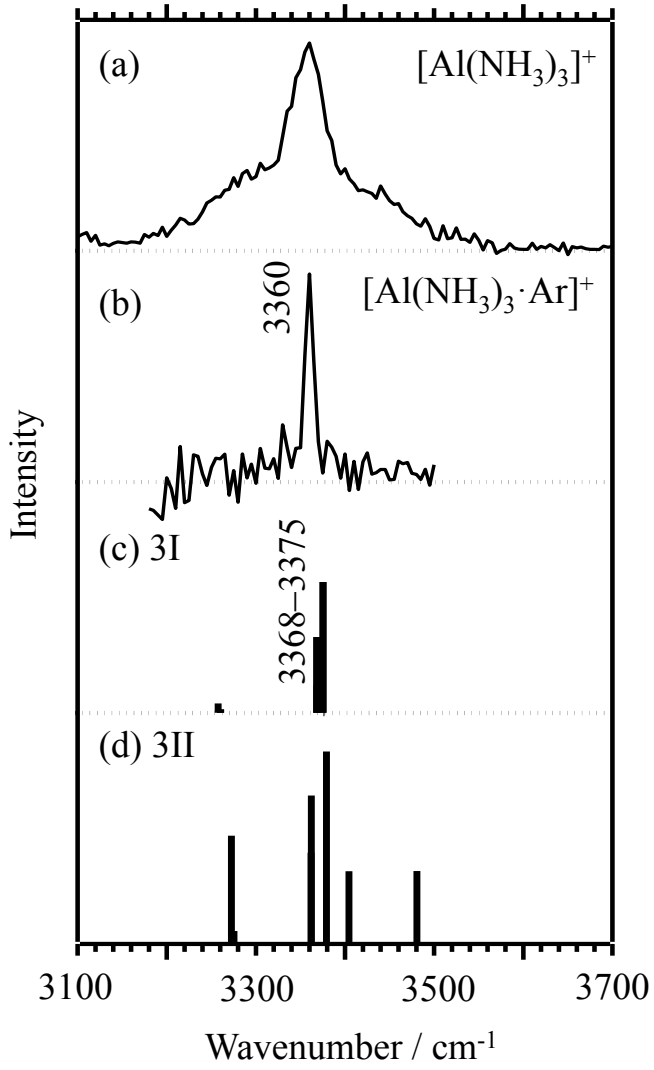

Fig. 3 Mune et al.

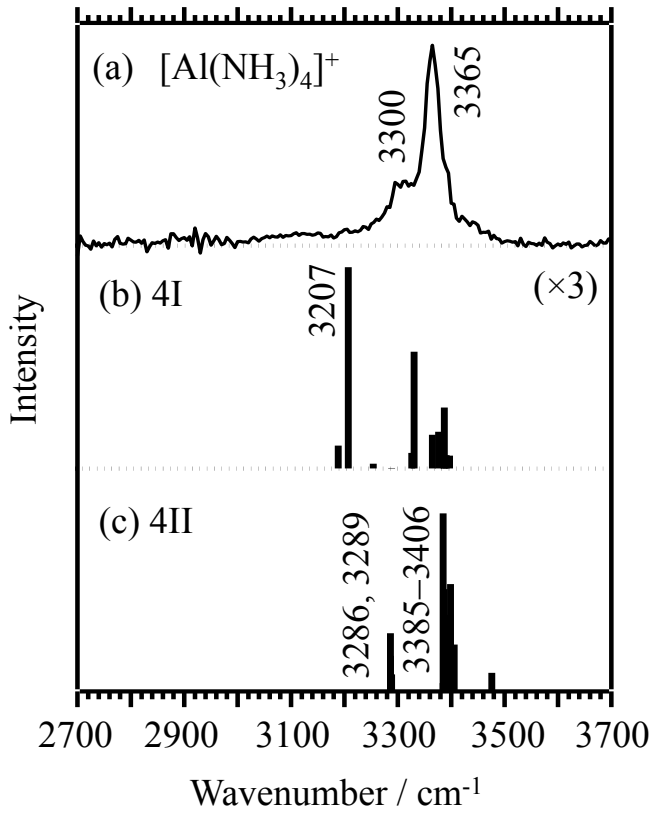

Fig. 4 Mune et al.

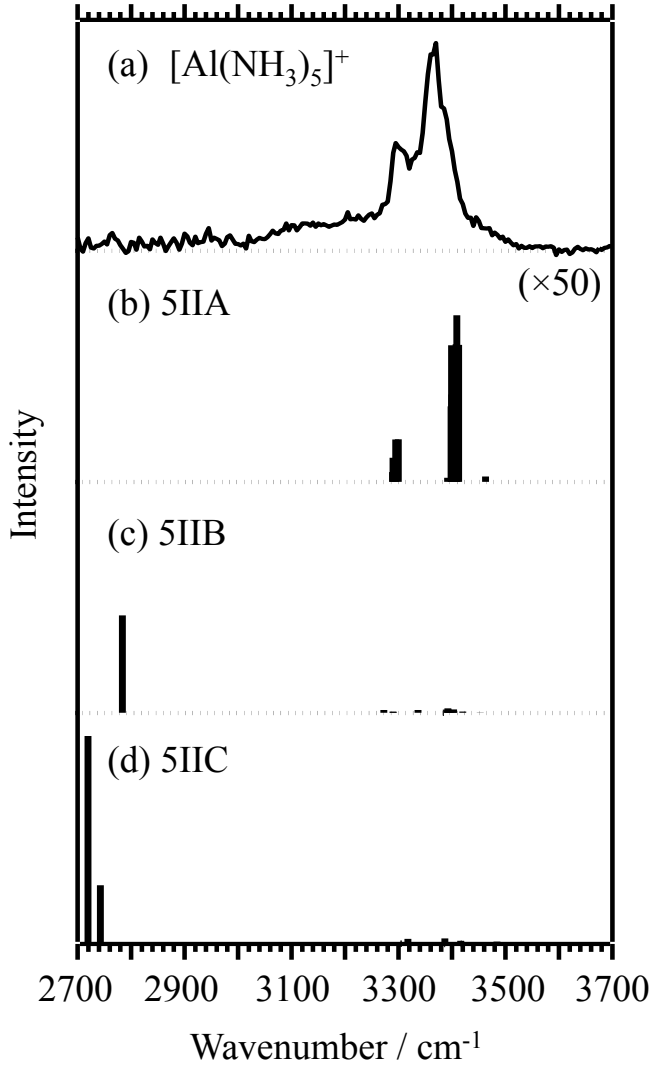

Fig. 5 Mune et al.